Organic Stealth Nanoparticles for Highly Effective *in Vivo* Near-Infrared Photothermal Therapy of Cancer

Liang Cheng, Kai Yang, Qian Chen, and Zhuang Liu*

Functional Nano & Soft Materials Laboratory (FUNSOM) and Jiangsu Key Laboratory for Carbon-Based Functional Materials & Devices, Soochow University, Suzhou, Jiangsu 215123, China

ABSTRACT In recent years, a wide range of near-infrared (NIR) light absorbing nanomaterials, mostly inorganic ones, have been developed for photothermal therapy (PTT) of cancer. In this work, we develop a novel organic PTT agent based on poly-(3,4-ethylenedioxythiophene):poly(4-styrenesulfonate) (PEDOT:PSS), a conductive polymer mixture with strong NIR absorbance, for *in vivo* photothermal treatment of cancer. After being layer-by-layer coated with charged polymers and then conjugated with branched polyethylene glycol (PEG), the obtained PEDOT:PSS-PEG nanoparticles are highly stable in the physiological environment and exhibit a stealth-like behavior after intravenous injection with a long blood circulation half-life. As a result, an extremely high *in vivo* tumor uptake of PEDOT:PSS-PEG attributed to the tumor-enhanced permeability and retention effect is observed. We further use PEDOT:PSS-PEG as a PTT agent for *in vivo* cancer treatment and realize excellent therapeutic efficacy in a mouse tumor model under NIR light irradiation at a low laser power density. Comprehensive blood tests and careful histological examination reveal no apparent toxicity of PEDOT:PSS-PEG to mice at our treated dose within 40 days. To our best knowledge, this work is the first to use systemically administrated conductive polymer nanoparticles for highly effective *in vivo* PTT treatment in animals and encourages further explorations of those organic nanomaterials for cancer theranostic applications.

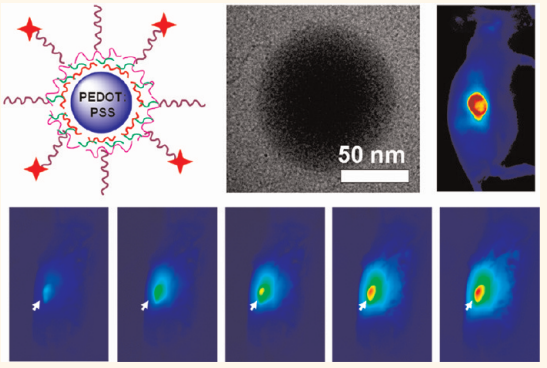

KEYWORDS: PEDOT:PSS · conductive polymer · organic nanoparticles · stealth nanoparticles · photothermal therapy

Photothermal therapy (PTT) is a hyperthermia therapeutic approach that employs photoabsorbing agents to burn cancer cells by heat generated from optical energy.[1−3] Compared with traditional cancer therapies such as radiotherapy and chemotherapy, PTT cancer treatment is highly selective and minimally invasive, as its therapeutic effect happens only at the tumor site with both light-absorber accumulation and localized laser exposure, without damaging normal tissues. A variety of nanomaterials, such as different gold nanostructures,[4−9] carbon nanomaterials (*e.g.*, carbon nanotubes, nanographene),[2,10−13] palladium nanosheets,[14] and copper sulfide nanoparticles,[15] which all show high absorbance in the tissue-transparent near-infrared (NIR) optical window (700−900 nm), have been widely explored by many research groups including ours as photothermal agents for PTT ablation of cancer. However, most of these currently used PTT agents were inorganic nanomaterials, which are nonbiodegradable and usually would remain in the body for long periods of time, raising concerns regarding their potential long-term toxicity.[16]

Organic nanoparticles, typically polymeric ones, have been extensively used in nanomedicine as drug/gene delivery carriers, many of which have already entered the clinic. Light-absorbing organic nanoparticles as PTT treatment agents, however, have been relatively less explored except for recent papers demonstrating the possibility of using polyaniline conductive polymers for photothermal killing of cancer cells[17] and porphysome organic nanoparticles for biophotonic imaging and therapy.[18] In our work here, we develop a novel PTT agent based on poly(3,4-ethylenedioxythiophene):poly(4-styrenesulfonate) (PEDOT:PSS), which is a widely used conductive polymer mixture in organic electronics[19−23] and shows strong absorbance in the NIR region, for highly effective *in vivo* photothermal ablation of tumors in a mouse model. *Via* a layer-by-layer (LBL) self-assembly approach, negatively charged PEDOT:PSS nanoparticles are first coated with positively charged poly(allylamine hydrochloride) (PAH)[24] and then negative charged poly(acrylic acid) (PAA). After

* Address correspondence to zliu@suda.edu.cn.

Received for review April 7, 2012 and accepted May 16, 2012.

Published online May 22, 2012
10.1021/nn301539m

cross-linking the two coating layers by amide formation, a branched polyethylene glycol[25] is further conjugated onto these nanoparticles, improving their physiological stability. The obtained PEGylated PEDOT:PSS (PEDOT:PSS-PEG) nanoparticles exhibit a "stealth-like" behavior with a long second phase blood circulation half-life of 21.4 ± 3.1 h and, as a result, extremely high tumor accumulation owing to the enhanced permeability and retention (EPR) effect of cancerous tumors. We further utilize the strong NIR optical absorption ability of PEDOT:PSS-PEG for *in vivo* photothermal therapy and achieve highly efficient tumor destruction by intravenous injection of PEDOT:PSS-PEG and laser irradiation of tumors at a low optical power density (0.5 W/cm^2). Moreover, no obvious sign of toxicity is observed for PEDOT:PSS-PEG-injected mice. Our work achieves *in vivo* photothermal treatment of cancer with excellent therapeutic efficacy using organic conductive nanoparticles and highlights the promise of using light-absorbing conductive polymers for phototherapy of cancer.

RESULTS AND DISCUSSION

PEDOT:PSS is a complex between the conjugated polymer PEDOT and the negatively charged polymer PSS. In aqueous phase, PEDOT:PSS forms water-soluble nanoparticles with diameters of ~80 nm.[19−23] In our study, PEDOT:PSS-PEG nanoparticles were synthesized from PEDOT:PSS through a LBL self-assembly procedure (Figure 1a). First, raw negatively charged PEDOT:PSS nanoparticles were modified by the cationic polymer PAH with a molecular weight (MW) of 15 kDa by electrostatic interaction, resulting in a positive charge for PEDOT:PSS. Second, anionic PAA (MW = 1.8 kDa) polymer was attached onto the surface of PEDOT:PSS/PAH again by electrostatic interaction and then cross-linked with the PAH layer by adding 1-ethyl-3-(3-dimethylaminopropyl)carbodiimide to trigger amide formation. Excess counter-charged polymer was added at each step to ensure the full coverage of the nanoparticle surface. The zeta potentials of nanoparticles increased from −40 mV for PEDOT:PSS to +24 mV for that of PEDOT:PSS/PAH and then decreased to −32 mV after PAA coating (Supporting Figure S1), indicating the successful LBL polymer adsorption on PEDOT:PSS nanoparticles. Lastly, an amine-terminated six-arm branched PEG (10 kDa) was conjugated to surface carboxyl groups on PEDOT:PSS/PAH/PAA nanoparticles *via* amide formation, obtaining PEDOT:PSS-PEG (PAH and PAA are omitted to be concise in this abbreviation) used in our following experiments. The composition of these complex nanoparticles was estimated to be (PEDOT:PSS):PAH/PAA:PEG = 1:0.8:1 by weight. While PEDOT:PSS/PAH/PAA rapidly precipitated in the presence of salts, PEDOT:PSS-PEG after PEG conjugation exhibited remarkably improved stability in various physiological solutions for several days including saline, cell medium, and serum (Supporting Figure S2), suggesting successful PEGylation of these nanoparticles. Amino groups on the branched-PEG termini were available for bioconjugation and fluorescent labeling.

The synthesized PEDOT:PSS-PEG nanoparticles showed relatively uniform sizes with an average diameter of 80−90 nm (Figure 1b) based on scanning electron microscope (SEM) and transmission electron microscope (TEM) images. As the number of polymer layers during the LBL assembly process increased, the sizes of the nanoparticles measured by dynamic light scattering (DLS) also slightly increased (Figure 1c), showing an average hydrodynamic diameter of ~130 nm for the final product PEDOT:PSS-PEG. Both PEDOT:PSS and PEDOT:PSS-PEG nanoparticles displayed high optical absorption in the NIR range with a peak at ~830 nm (Figure 1d). To verify the potential of using PEDOT:PSS-PEG as a PTT agent, a PEDOT:PSS-PEG solution (0.1 mg/mL) was exposed to an 808 nm NIR laser at a power density of 1 W/cm^2. When exposed to the laser, the temperature of the PEDOT:PSS-PEG solution increased rapidly, while pure water showed little change (Figure 1e). Notably, under 808 nm laser irradiation, the photostability of PEDOT:PSS-PEG was much better than that of gold-based nanomaterials such as Au nanorods, whose absorbance peak diminished under laser irradiation at the same conditions, possibly due to the detachment of conjugated PEG and/or the "melting effect"[8,26] after a long period of laser exposure (Supporting Figures S3, S4).

We next tested our PEDOT:PSS-PEG in biological systems. Standard cell viability tests were carried out first to test any potential *in vitro* toxicity of PEDOT:PSS-PEG and PEDOT:PSS solutions to two different cell lines including the murine breast cancer 4T1 cell line and the human embryonic kidney 293T cell line. It was found that PEDOT:PSS-PEG, even at high concentrations up to 0.2 mg/mL, exhibited no appreciable negative effect on the viability of cells after exposure for 24 h, while PEDOT:PSS without PEGylation was dose-dependently toxic to the two types of cells (Supporting Figure S5). Our results suggest that the cytotoxicity of conductive polymer nanoparticles was closely associated with their surface chemistry, and the PEG coating could remarkably improve the biocompatibility of our nanoparticles and possibly reduce their nonspecific cell internalization, as indicated by the long blood half-life of these nanoparticles uncovered in the followed studies.

The *in vivo* behaviors of PEDOT:PSS-PEG nanoparticles were then investigated. Cy5, a commonly used fluorescent dye, was used to label the PEG termini of PEDOT:PSS-PEG (Figure 1a, Supporting Figure S6). It was estimated each PEG polymer on PEDOT:PSS-PEG nanoparticles was labeled with ~0.7 Cy5 molecule based on the absorbance of Cy5. The obtained

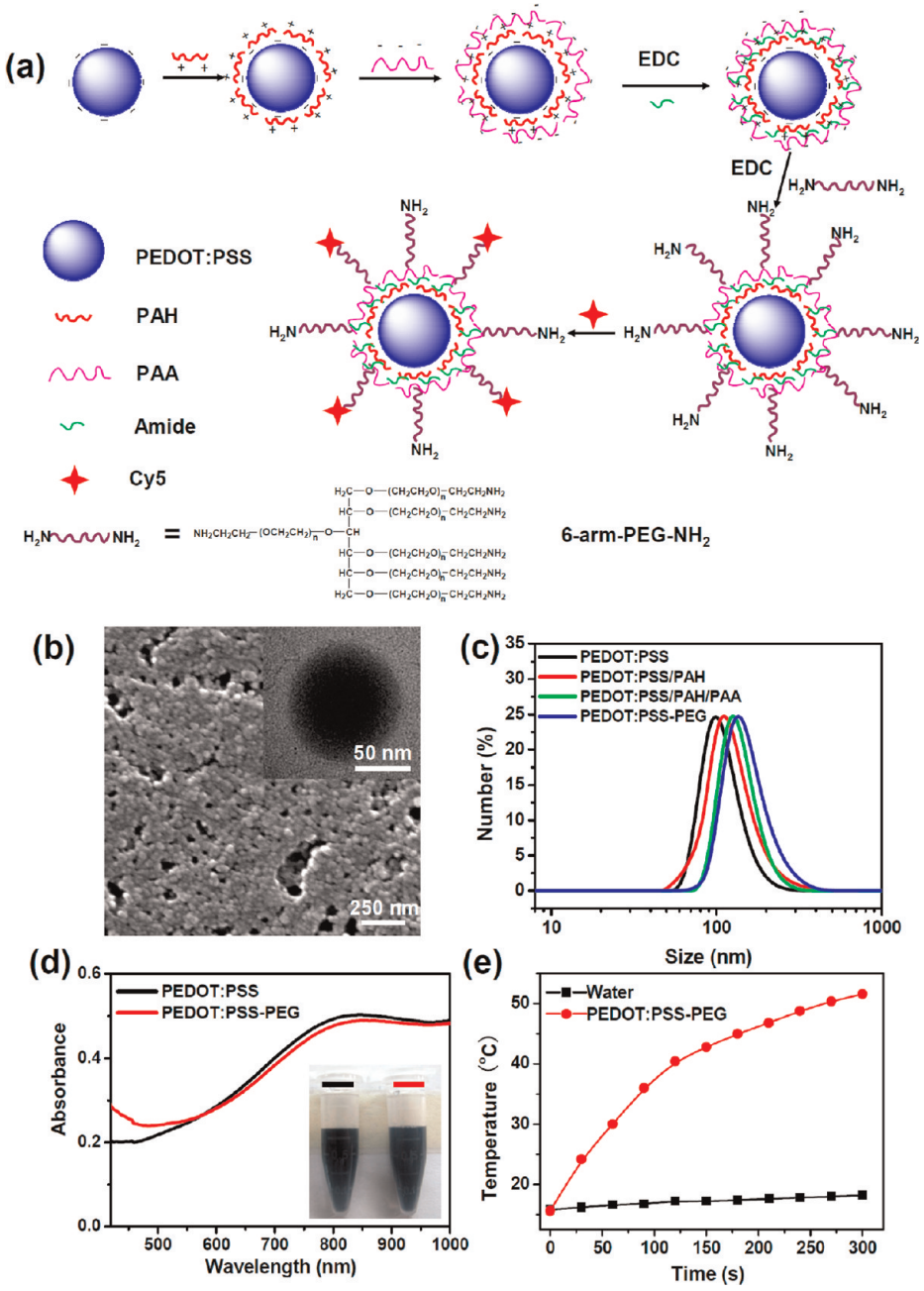

Figure 1. PEDOT:PSS-PEG synthesis and characterization. (a) Scheme showing the fabrication process of PEDOT:PSS-PEG. Note that a linear structure is drawn for simplification purposes to represent the branched six-arm-PEG-amine. (b) SEM image of PEODT:PSS-PEG nanoparticles deposited on a silicon substrate. Inset: TEM image of a single PEDOT:PSS-PEG nanoparticle. (c) DLS-measured diameters of PEDOT:PSS nanoparticles after step-by-step polymer coatings. (d) UV–vis–NIR spectra of PEDOT:PSS and PEDOT:PSS-PEG solutions at a concentration of 0.02 mg/mL. Inset: Photo of PEDOT:PSS (left) and PEDOT:PSS-PEG (right) solutions at a concentration of 0.1 mg/mL in water. (e) Heating curves of pure water and PEDOT:PSS-PEG (0.1 mg/mL) under 808 nm laser irradiation at a power density of 1 W/cm^2.

PEDOT:PSS-PEG-Cy5 (200 μL of 1 mg/mL per mouse, or a dose of 10 mg/kg) was intravenously injected into Balb/c mice with blood drawn at certain time intervals post-injection (pi) (Figure 2a). The blood was solubilized by a lysis buffer and measured by a fluorometer to determine the PEDOT:PSS-PEG-Cy5 concentrations. The blood circulation of PEDOT:PSS-PEG-Cy5 followed a typical two-compartment model.[8] After a rapid decay with the first phase (distribution phase, usually a rapid decline) half-life of 0.3 $\pm$ 0.24 h, those nanoparticles in circulating blood exhibited a long second phase (elimination phase, the predominant process for drug clearance) half-life of 21.4 $\pm$ 3.1 h. The long blood circulation makes PEDOT:PSS-PEG "stealth nanoparticles"[27,28] and is likely due to the condensed PEG coating on the nanoparticles, which delays their macrophage clearance in reticuloendothelial systems (RES), favorable for enhanced tumor targeting by the EPR effect.

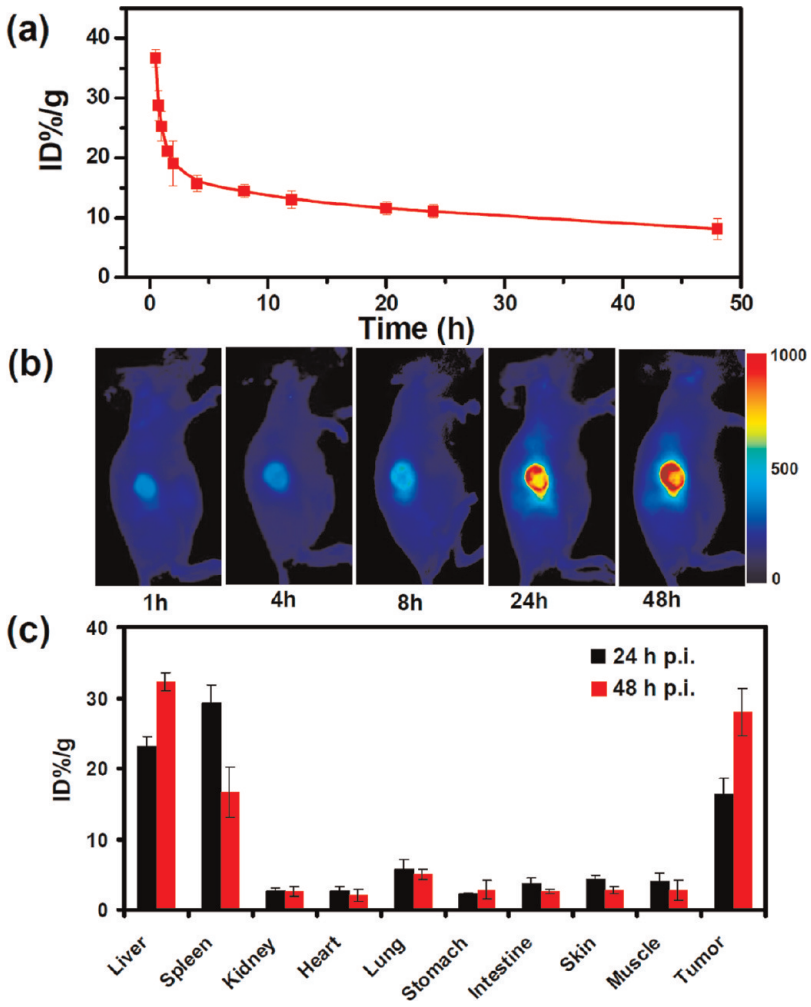

Figure 2. *In vivo* **behaviors of PEDOT:PSS-PEG-Cy5 after intravenous injection (dose = 10 mg/kg). (a) Blood circulation curve of PEDOT:PSS-PEG-Cy5 after intravenous injection as determined by measuring Cy5 fluorescence in the blood at different time points post-injection. The unit is percentage of injected dose per gram tissue (% ID/g). (b)** *In vivo* **fluorescence images of 4T1 tumor bearing Balb/c mice at different time points post-injection of PEDOT:PSS-PEG-Cy5. The autofluorescence of the mouse was removed by spectral unmixing. (c) Biodistribution of PEDOT:PSS-PEG-Cy5 in mice determined by the Cy5 fluorescence from diluted tissue lysates.**

Next, Balb/c mice bearing 4T1 murine breast cancer tumors were intravenously injected with PEDOT:PSS-PEG-Cy5 (200 μL of a 1 mg/mL solution for each mouse) and then spectrally imaged by a Maestro EX *in vivo* fluorescence imaging system (CRi, Inc.) (Figure 2b). The mouse autofluorescence was removed by spectral unmixing using the Maestro software, leaving pure Cy5 fluorescence shown in Figure 2b. It was found that PEDOT:PSS-PEG-Cy5 tended to be enriched in the tumor over time, with prominent uptake of nanoparticles observed in the tumor at 48 h pi. Control experiments uncovered that the majorities of free Cy5 (MW = 792 Da) and Cy5-labeled PEG (MW = 10 kDa) were excreted within 4−8 h by fast renal clearance (Supporting Figure S7), suggesting that the observed fluorescent signals in PEDOT:PSS-PEG-Cy5-injected mice were indeed from the labeled PEDOT:PSS-PEG nanoparticles rather than free or detached fluorescent dyes.

In order to understand the *in vivo* biodistribution of PEDOT:PSS-PEG, 4T1 tumor-bearing Balb/c mice injected with PEDOT:PSS-PEG (200 μL, 1 mg/mL) were sacrificed at 24 and 48 h pi. The major organs of the mice (n = 4 per group) were weighed and solubilized by a lysis buffer. The obtained homogenized tissue lysates were diluted and measured by a fluorometer to quantitatively determine the PEDOT:PSS-PEG-Cy5 concentrations (see Experimental Section for detailed sample preparation). Organs from a control mouse without injection of nanoparticles were collected and used as controls to subtract the autofluorescence background in various tissues. High levels of PEDOT:PSS-PEG-Cy5 were observed in the tumor as well as RES organs such as liver and spleen (Figure 2c). The latter were not seen in *in vivo* fluorescent images due to the tissue penetration limit of Cy5 fluorescence. The tumor uptake was measured to be 16.33% and 28.02% ID/g, at 24 and 48 h pi, respectively. The high tumor accumulation

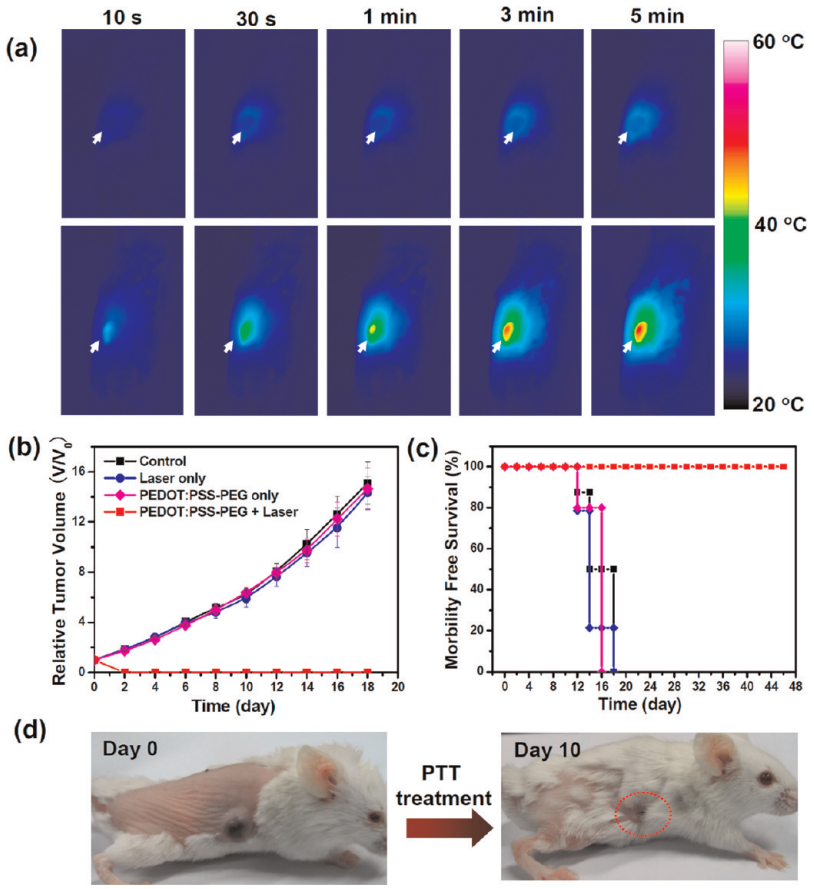

Figure 3. *In vivo* **photothermal therapy using PEDOT:PSS-PEG. (a) Infrared thermal images of 4T1 tumor-bearing mice without (upper row) or with (lower row) intravenous injection of PEDOT:PSS-PEG (10 mg/kg, 48 h pi) under 808 nm laser irradiation taken at different time intervals. The laser power density was 0.5 W/cm^2. Arrows point to the tumors. (b) Growth of 4T1 tumors in different groups of mice after treatment. The relative tumor volumes were normalized to their initial sizes. For the treatment group, 10 mice injected with PEDOT:PSS-PEG at 48 h pi were exposed to the 808 nm laser (0.5 W/cm^2, 5 min). The other three groups of mice were used as controls: untreated (control, *n* = 8); laser only without PEDOT:PSS-PEG injection (laser only, *n* = 14); injected with PEDOT:PSS-PEG but without laser irradiation (PEDOT:PSS-PEG only, *n* = 10). Error bars were based on standard deviations. (c) Survival curves of mice after various treatments as indicated in (b). PEDOT:PSS-PEG-injected mice after PTT treatment showed 100% survival ratio over 45 days. (d) Representative photos of a PEDOT:PSS-PEG-injected mouse at day 0 before PTT treatment and at day 10 after treatment. The tumor color turned obviously darker after PEDOT:PSS-PEG injection at 48 h pi (left). Complete tumor elimination was achieved after PTT treatment (right).**

of PEDOT:PSS-PEG could be due to the EPR effect in cancerous tumors with tortuous and leaky vasculatures, which tend to trap materials in the nanosize range.

Motivated by the high tumor accumulation of PEDOT:PSS-PEG and its strong NIR optical absorption, we then carried out an *in vivo* photothermal therapy using PEDOT:PSS-PEG. For *in vivo* monitoring of the photothermal effect generated from PEDOT:PSS-PEG, an infrared thermal mapping apparatus was used to record the temperature change in the tumor area under irradiation by a NIR laser. After being intravenously injected with PEDOT:PSS-PEG solution (200 μL, 1 mg/mL) for 48 h, mice bearing 4T1 tumors were anesthetized and exposed to a 808 nm laser at the power density of 0.5 W/cm^2. Under irradiation, the tumor surface temperature obviously increased from ~30 to ~51 °C within 5 min (Figure 3a). In comparison, the tumor temperature of mice without PEDOT:PSS-PEG injection under the same laser irradiation showed little change.

The therapeutic effect after PTT treatment was further investigated. Ten mice bearing a 4T1 tumor on their back were intravenously injected with PEDOT:PSS-PEG (200 μL, 1 mg/mL). At 48 h pi, the tumor of each mouse in the treatment group was exposed to an 808 nm laser at a power density of 0.5 W/cm^2 for 5 min. Three other groups including untreated mice (control, *n* = 8), mice exposed to the laser (laser only, *n* = 14), and PEDOT:PSS-PEG-injected mice without laser irradiation (PEDOT:PSS-PEG, *n* = 10) were used as the controls. Tumor sizes were measured every 2 days after treatment. After laser irradiation, tumors on PEDOT:PSS-PEG-injected mice were completely eliminated one day post-irradiation (Figure 3b, d). In marked contrast, neither laser irradiation at the current power density nor PEDOT:PSS-PEG injection by itself affected the tumor growth (Figure 3b). While mice in the three control groups showed average life spans of 16–18 days, mice in the treated group

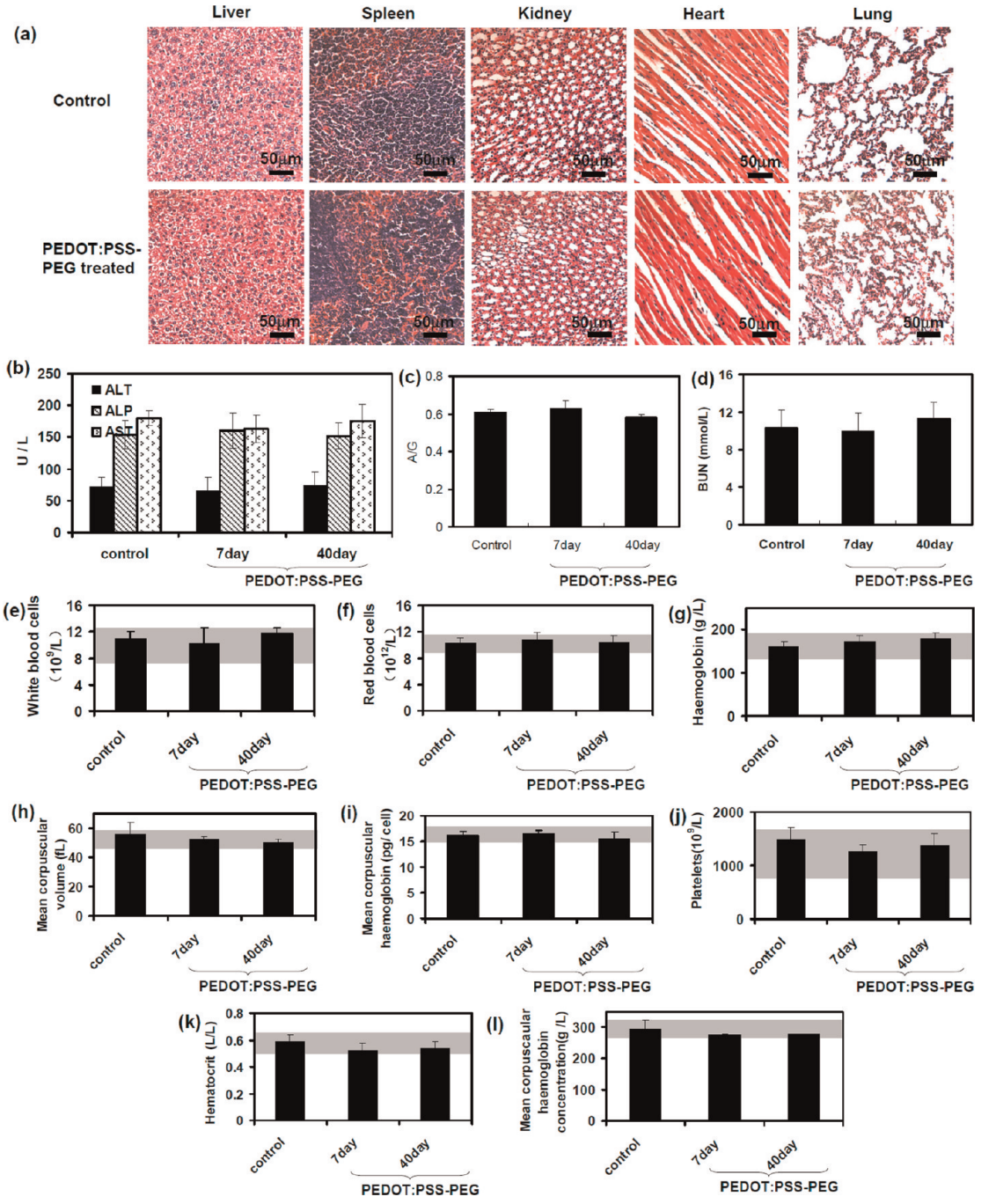

Figure 4. *In vivo* toxicology study. (a) H&E stained images of major organs. Mice with PEDOT:PSS-PEG injection that survived after photothermal therapy (with tumors eliminated) were sacrificed 45 days after treatment. No noticeable abnormality was observed in major organs including liver, spleen, kidney, heart, and lung. (b–d) Serum biochemistry data. Healthy female Balb/c mice intravenously injected with PEDOT:PSS-PEG (dose = 10 mg/kg) were sacrificed at 7 days and 40 days pi for blood collection. Untreated healthy mice were used as the control. (b) Levels of liver function markers including alanine aminotransferase (ALT), aspartate aminotransferase (AST), and alkaline phosphatase (ALP) in the blood of different groups of mice. (c) Albumin/globin ratios in different groups of mice. (d) Blood urea nitrogen (BUN) levels. No hepatic disorder was induced by PEDOT:PSS-PEG as revealed by serum biochemistry data. Complete blood panel. Blood levels of white blood cells (e), red blood cells (f), hemoglobin (g), mean corpuscular volume (h), mean corpuscular hemoglobin (i), platelets (j), hematocrit (k), and mean corpuscular hemoglobin concentration (l) of control and PEDOT:PSS-PEG-treated mice. Gray areas: reference normal ranges of various hematology data for healthy female Balb/c mice. All blood chemistry and hematological data were within the normal range. Statistics were based on five mice per data point. Reference ranges of hematology data of healthy female Balb/c mice were obtained from Charles River Laboratories: http://www.criver.com/EN-US/PRODSERV/BYTYPE/RESMODOVER/RESMOD/Pages/BALBcMouse.aspx (last accessed March 4, 2012).

(PEDOT:PSS-PEG + laser) were tumor-free after treatment and survived over 45 days without a single death (Figure 3c, d). Our results suggested that PEDOT:PSS-PEG was a powerful agent for *in vivo* photothermal ablation of cancer.

Lastly, the potential *in vivo* toxicity of PEDOT:PSS-PEG was also investigated. We carefully supervised the behaviors of PEDOT:PSS-PEG-injected (10 mg/kg) Balb/c mice in our experiments after PTT treatment and tumor ablation and noticed no obvious sign of toxic effect within 45 days. No significant body weight drop was noted for mice in all four groups (Supporting Figure S8). Mice were sacrificed at day 45 for careful necropsy, which uncovered neither noticeable abnormality nor metastatic tumors. The major organs of the mice were sliced and stained by hematoxylin and eosin (H&E) for histology analysis (Figure 4a). Despite the high RES uptake of PEDOT:PSS-PEG in liver and spleen, no noticeable organ damage or inflammatory lesion was observed in all major organs of mice 45 days after PTT treatment.

To further study the potential toxicology of PEDOT:PSS-PEG in relatively short and long terms, a serum biochemistry assay and complete blood panel test were carried on PEDOT:PSS-PEG-injected (10 mg/kg) healthy Balb/c mice at days 7 and 40 pi. Excitingly, all measured parameters fell within normal ranges (Figure 4b–l). Our results collectively evidence that PEDOT:PSS-PEG nanoparticles are not noticeably toxic *in vivo* to mice at least at our tested dose. However, much more effort is still required to systematically examine any potential long-term toxicity of our organic nanoparticles at various doses to animals.

CONCLUSION

In summary, PEGylated organic nanoparticles based on PEDOT:PSS conductive polymers are fabricated and used for highly effective *in vivo* PTT treatment of cancer in animal experiments. Using the LBL method, PEDOT:PSS polymeric nanoparticles were step-by-step coated with charged polymers and then conjugated with PEG, obtaining PEDOT:PSS-PEG with excellent compatibility in physiological environments. With a long blood circulation half-life, the stealth PEDOT:PSS-PEG nanoparticles show surprisingly high *in vivo* tumor uptake by the EPR effect after intravenous injection and appear to be an excellent PTT agent for tumor ablation, without rendering any obvious toxicity to the treated animals. This work for the first time explores the *in vivo* behaviors, applications, and potential toxicity of conductive polymers in animal models and, most importantly, realizes *in vivo* photothermal therapy in animals with excellent therapeutic efficacy under a low laser power using systemically administrated organic nanoparticles. Additional functionalities in imaging and combined therapies may also be achieved by carefully designing and engineering these polymeric nanoparticles. Conjugation of tumor-homing ligands on these nanoparticles may further enhance their tumor-targeting capability. Although we are still not clear whether or how PEDOT:PSS-PEG would degrade in biological systems and its long-term excretion, metabolism, and toxicology need many more careful investigations, our results show promise for the use of conjugated polymeric nanoparticles for PTT cancer treatment and encourage future research to develop biodegradable light-absorbing organic nanomaterials for photothermal cancer therapy with real potential in the clinic.

EXPERIMENTAL SECTION

Synthesis of PEDOT:PSS-PEG. PEDOT:PSS conductive polymer solution (CLEVIOS PH1000) was purchased from Baier Chemical Industrial Co. PEGylated PEDOT:PSS was synthesized through the LBL method.

First, 5 mL (0.5 mg/mL) of PEDOT:PSS solution was dropwisely added into 5 mL of PAH solution (MW = 15 000, 1 mg/mL) under ultrasonication for 30 min. After stirring for 6 h, a PEDOT:PSS/PAH solution was obtained and purified by filtration through 100 kDa molecular weight cut-off (MWCO) filters (Millipore) to remove excess PAH.

Second, the above PEDOT:PSS/PAH solution was dropwisely added into 5 mL of PAA solution (MW = 1800, 2 mg/mL) under ultrasonication for 30 min and then stirred for 6 h. The solution was purified by filtration through 100 kDa MWCO filters two times. After adjusting the pH to 7.4, 5 mg of *N*-(3-dimethylaminopropyl-*N*′-ethylcarbodiimide) hydrochloride (EDC, Fluka Inc.) was added into this solution to induce cross-linking between PAH and PAA layers on the nanoparticles. The reaction was allowed to occur overnight, yielding a PEDOT:PSS/PAH/PAA solution, which was purified by filtration through 100 kDa MWCO filters.

Lastly, to prepare PEDOT:PSS-PEG, a PEDOT:PSS/PAH/PAA solution was sonicated to obtain a clear solution. A solution of six-arm PEG-amine (Sunbio Inc. P6AM-10) at 2 mg/mL was added into the PEDOT:PSS/PAH/PAA solution, and the mixture was sonicated for 30 min. Then 10 mg of EDC was added to the mixture, and the pH adjusted to 7.4 by phosphate buffer. The reaction was allowed to sit overnight, yielding a PEDOT:PSS-PEG solution, which was purified by filtration and stored at 4 °C for future use.

Fluorescent Labeling of PEDOT:PSS-PEG. After removing excess PEG by filtration and repeated washing, the purified PEDOT:PSS-PEG (0.5 mg/mL) was reacted with an amine reactive dye, Cy5-SE (Fanbo Biochemicals Co., Ltd. Beijing, China), at 0.1 mg/mL in a pH 7.4 phosphate buffer (0.02 M). The reaction was allowed to sit overnight at room temperature in the dark. Excess dye molecules were removed by centrifugal filtration through 100 kDa MWCO filters and washed away with water more than three times until no noticeable color remained in the filtrate solution.

Tumor Model. 4T1 murine breast cancer cells were cultured under the standard conditions recommended by American Type Culture Collection (ATCC). Balb/c mice were obtained from Suzhou Belda Bio-Pharmaceutical Co., Ltd. and used under protocols approved by Soochow University Laboratory Animal Center. The 4T1 tumors were generated by subcutaneous injection of 5×10^6 cells in ~100 μL of serum-free RMPI-1640 medium onto the back of female Balb/c mice.

Characterization. The scanning electron microscopy images were taken by using a FEI Quanta 200F scanning electron

microscope. Transmission electron microscopy images of the nanocrystals were obtained using a Philips CM300 transmission electron microscope operating at an acceleration voltage of 200 kV. Fluorescence spectra were obtained on a FluoroMax 4 luminescence spectrometer (HORIBA Jobin Yvon) with an excitation source of the xenon lamp in the spectrometer. UV−vis−NIR spectra were acquired by using a PerkinElmer Lambda 750 UV−vis−NIR spectrophotometer.

***In Vivo* Fluorescence Imaging.** Tumor-bearing mice were intravenously injected with 200 μL of 1 mg/mL PEDOT:PSS-PEG-Cy5 and imaged using the Maestro *in vivo* fluorescence imaging system (CRi Inc.). Visible red light with a central wavelength of 605 nm was used as the excitation source. *In vivo* spectral imaging from 640 to 800 nm (10 nm steps) was carried out with an exposure time of 75 ms for each image frame. Autofluorescence (particularly from food residues in the stomach and intestine) was removed by using the spectral unmixing software.

Blood Circulation. Blood circulation was measured by drawing ~10 μL of blood from the tail vein of 4T1 tumor bearing Balb/c mice post-injection of PEDOT:PSS-PEG-Cy5. Each blood sample was dissolved in 1 mL of lysis buffer (1% SDS, 1% Triton X-100, 40 mM Tris acetate). The concentration of PEDOT:PSS-PEG-Cy5 in the blood was determined by the fluorescence spectrum of each solubilized blood sample using a FluoroMax 4 fluorometer (Horiba Jobin Yvon, France) with the excitation and emission peaks at ~605 and ~670 nm. A series of dilutions of PEDOT:PSS-PEG-Cy5 solutions were measured to obtain a standard calibration curve. Blank blood sample without PEDOT:PSS-PEG-Cy5 injection was measured to determine the blood autofluorescence level, which was subtracted from the fluorescence intensities of injected samples during the concentration calculation. The PEDOT:PSS-PEG-Cy5 is presented as the percentage of injected dose per gram of tissue (% ID/g).

Biodistribution Measurement. For biodistribution study, 4T1 tumor-bearing mice (tumor size ~100 mm^3) were sacrificed at 24 and 48 h post-injection of PEDOT:PSS-PEG-Cy5. The organs/tissues were weighed and homogenized in the lysis buffer (the same as the above used in the blood circulation experiment) with a PowerGen homogenizer (Fisher Scientific). Clear homogeneous tissue solutions were obtained and diluted 10−100 times to avoid significant light scattering and self-quenching during fluorescence measurement. The fluorescence intensities of both standard samples and real tissue samples were all adjusted to be in the linear range by appropriate dilution. The sample was measured in triplicate to ensure reproducibility and measurement accuracy. The biodistribution of PEDOT:PSS-PEG in various organs of the mice was then calculated and plotted in units of % ID/g.

Photothermal Therapy. An optical fiber coupled 808 nm high-power diode-laser (Hi-Tech Optoelectronics Co., Ltd. Beijing, China) was used to irradiate tumors during our experiments. For photothermal treatment, the laser beam with a diameter of ~10 mm was focused on the tumor area at the power density of 0.5 W/cm^2 for 5 min. Infrared thermal images were taken by an ICI 7320 Pro thermal imaging camera. The tumor sizes were measured by a caliper every other day and calculated as volume = (tumor length) × (tumor width)^2/2. Relative tumor volumes were calculated as V/V_0 (V_0 is the tumor volume when the treatment was initiated).

Histology Analysis. Forty-five days after injection of PEDOT:PSS-PEG (dose = 10 mg/kg), three mice from the treatment group and three age-matched female Balb/c control mice (without any injection of PEDOT:PSS-PEG) were sacrificed by CO_2 asphyxiation for necropsy. Major organs from these mice were harvested, fixed in 10% neutral buffered formalin, processed routinely into paraffin, sectioned at 8 μm, stained with hematoxylin and eosin (H&E), and examined by a digital microscope (Leica QWin). Examined tissues include liver, spleen, kidney, heart, lung, and intestine.

Blood Analysis. Ten healthy Balb/c mice were injected with 200 μL of 1 mg/mL PEDOT:PSS-PEG (a dose of 10 mg/kg). The other five mice were used as the untreated controls. Mice were sacrificed to collect the blood (0.8 mL) for blood biochemistry assay and complete blood panel test at 7 and 45 days post-injection of PEDOT:PSS-PEG. The serum chemistry data and complete blood panel were measured in Shanghai Research Center for Biomodel Organism.

Conflict of Interest: The authors declare no competing financial interest.

Acknowledgment. This work was partially supported by the National Natural Science Foundation of China (51002100, 51072126), the National "973" Program of China (2012CB932601, 2011CB911002), and a Project Funded by the Priority Academic Program Development of Jiangsu Higher Education Institutions. L.C. was supported by the Innovation Program of Graduate Students in Jiangsu Province (CX10B_036Z). We thank Prof. Jun Wang in the University of Science and Technology of China for offering us access to the IR thermal camera, and Prof. Baoquan Sun at FUNSOM in Soochow University for helpful discussions.

Supporting Information Available: PEDOT:PSS-PEG characterization data, cell toxicity, and various control fluorescence imaging data are available free of charge via the Internet at http://pubs.acs.org.

REFERENCES AND NOTES

1. Lal, S.; Clare, S. E.; Halas, N. J. Nanoshell-Enabled Photothermal Cancer Therapy: Impending Clinical Impact. *Acc. Chem. Res.* **2008**, *41*, 1842–1851.
2. Robinson, J. T.; Tabakman, S. M.; Liang, Y.; Wang, H.; Casalongue, H. S.; Vinh, D.; Dai, H. Ultrasmall Reduced Graphene Oxide with High Near-Infrared Absorbance for Photothermal Therapy. *J. Am. Chem. Soc.* **2011**, *133*, 6823–6831.
3. Liu, H.; Chen, D.; Li, L.; Liu, T.; Tan, L.; Wu, X.; Tang, F. Multifunctional Gold Nanoshells on Silica Nanorattles: A Platform for the Combination of Photothermal Therapy and Chemotherapy with Low Systemic Toxicity. *Angew. Chem., Int. Ed.* **2011**, *50*, 891–895.
4. Maltzahn, G. v.; Park, J.-H.; Agrawal, A.; Bandaru, N. K.; Das, S. K.; Sailor, M. J.; Bhatia, S. N. Computationally Guided Photothermal Tumor Therapy Using Long-Circulating Gold Nanorod Antennas. *Cancer Res.* **2009**, *69*, 3892–3900.
5. Ke, H.; Wang, J.; Dai, Z.; Jin, Y.; Qu, E.; Xing, Z.; Guo, C.; Yue, X.; Liu, J. Gold-Nanoshelled Microcapsules: A Theranostic Agent for Ultrasound Contrast Imaging and Photothermal Therapy. *Angew. Chem., Int. Ed.* **2011**, *50*, 3017–3021.
6. Liu, H.; Liu, T.; Wu, X.; Li, L.; Tan, L.; Chen, D.; Tang, F. Targeting Gold Nanoshells on Silica Nanorattles: A Drug Cocktail to Fight Breast Tumors *via* a Single Irradiation with Near-Infrared Laser Light. *Adv. Mater.* **2012**, 10.1002/adma.201103343.
7. Cheng, L.; Yang, K.; Li, Y.; Chen, J.; Wang, C.; Shao, M.; Lee, S.-T.; Liu, Z. Facile Preparation of Multifunctional Upconversion Nanoprobes for Multi-modal Imaging and Dual-targeted Photothermal Therapy. *Angew. Chem., Int. Ed.* **2011**, *50*, 7385–7390.
8. Cheng, L.; Yang, K.; Li, Y.; Zeng, X.; Shao, M.; Lee, S.-T.; Liu, Z. Multifunctional Nanoparticles for Upconversion Luminescence/MR Multimodal Imaging and Magnetically Targeted Photothermal Therapy. *Biomaterials* **2012**, *33*, 2215–2222.
9. Dong, W.; Li, Y.; Niu, D.; Ma, Z.; Gu, J.; Che, Y.; Zhao, W.; Liu, X.; Liu, C.; Shi, J. Facile Synthesis of Monodisperse Superparamagnetic Fe_3O_4 Core@hybrid@Au Shell Nanocomposite for Bimodal Imaging and Photothermal Therapy. *Adv. Mater.* **2011**, *23*, 5392–5397.
10. Liu, X.; Tao, H.; Yang, K.; Zhang, S.; Lee, S.-T.; Liu, Z. Optimization of Surface Chemistry on Single-Walled Carbon Nanotubes for *in Vivo* Photothermal Ablation of Tumors. *Biomaterials* **2011**, *32*, 144–151.
11. Robinson, J. T.; Welsher, K.; Tabakman, S. M.; Sherlock, S. P.; Wang, H.; Luong, R.; Dai, H. High Performance *In Vivo* Near-IR (>1 μm) Imaging and Photothermal Cancer Therapy with Carbon Nanotubes. *Nano Res.* **2010**, *3*, 779–793.
12. Yang, K.; Zhang, S.; Zhang, G.; Sun, X.; Lee, S.-T.; Liu, Z. Graphene in Mice: Ultrahigh *in Vivo* Tumor Uptake and

Efficient Photothermal Therapy. *Nano Lett.* **2010**, *10*, 3318–3323.
13. Yang, K.; Wan, J.; Zhang, S.; Tian, B.; Zhang, Y.; Liu, Z. The Influence of Surface Chemistry and Size of Nanoscale Graphene Oxide on Photothermal Therapy of Cancer Using Ultra-low Laser Power. *Biomaterials* **2012**, *33*, 2206–2214.
14. Huang, X.; Tang, S.; Mu, X.; Dai, Y.; Chen, G.; Zhou, Z.; Ruan, F.; Yang, Z.; Zheng, N. Freestanding Palladium Nanosheets with Plasmonic and Catalytic Properties. *Nat. Nanotechnol.* **2011**, *6*, 28–32.
15. Tian, Q.; Tang, M.; Sun, Y.; Zou, R.; Chen, Z.; Zhu, M.; Yang, S.; Wang, J.; Wang, J.; Hu, J. Hydrophilic Flower-Like CuS Superstructures as an Efficient 980 nm Laser-Driven Photothermal Agent for Ablation of Cancer Cells. *Adv. Mater.* **2011**, *23*, 3542–3547.
16. Sharifi, S.; Behzadi, S.; Laurent, S.; Forrest, M. L.; Stroeve, P.; Mahmoudi, M. Toxicity of Nanomaterials. *Chem. Soc. Rev.* **2012**, *41*, 2323–2343.
17. Yang, J.; Choi, J.; Bang, D.; Kim, E.; Lim, E. K.; Park, H.; Suh, J. S.; Lee, K.; Yoo, K. H.; Kim, E. K.; Huh, Y. M.; Haam, S. Convertible Organic Nanoparticles for Near-Infrared Photothermal Ablation of Cancer Cells. *Angew. Chem., Int. Ed.* **2011**, *50*, 441–444.
18. Lovell, J. F.; Jin, C. S.; Huynh, E.; Jin, H.; Kim, C.; Rubinstein, J. L.; Chan, W. C. W.; Cao, W.; Wang, L.; Zheng, G. Porphysome Nanovesicles Generated by Porphyrin Bilayers for Use as Multimodal Biophotonic Contrast Agents. *Nat. Mater.* **2011**, *10*, 324–332.
19. Lefebvre, M.; Qi, Z.; Rana, D.; Pickup, P. G. Chemical Synthesis, Characterization, and Electrochemical Studies of Poly(3,4-ethylenedioxythiophene)/Poly(styrene-4-sulfonate) Composites. *Chem. Mater.* **1999**, *11*, 262–268.
20. Yun, J. M.; Yeo, J. S.; Kim, J.; Jeong, H. G.; Kim, D. Y.; Noh, Y. J.; Kim, S. S.; Ku, B. C.; Na, S. I. Solution-Processable Reduced Graphene Oxide as a Novel Alternative to PEDOT:PSS Hole Transport Layers for Highly Efficient and Stable Polymer Solar Cells. *Adv. Mater.* **2011**, *23*, 4923–4928.
21. Vosgueritchian, M.; Lipomi, D. J.; Bao, Z. Highly Conductive and Transparent PEDOT:PSS Films with a Fluorosurfactant for Stretchable and Flexible Transparent Electrodes. *Adv. Funct. Mater.* **2011**, *22*, 421–428.
22. Jørgensen, M.; Norrman, K.; Krebs, F. C. Stability/Degradation of Polymer Solar Cells. *Sol. Energy Mater. Lett.* **2008**, *92*, 686–714.
23. Khodagholy, D.; Doublet, T.; nkel, M. G.; Quilichini, P.; Ismailova, E.; Leleux, P.; Herve, T.; Sanaur, S.; Bernard, C.; Malliaras, G. G. Highly Conformable Conducting Polymer Electrodes for *in Vivo* Recordings. *Adv. Mater.* **2011**, *23*, 268–272.
24. Huang, S. K.; Mayhew, E.; Gilani, S.; Lasic, D. D.; Martin, F. J.; Papahadjopoulos, D. Pharmacokinetics and Therapeutics of Sterically Stabilized Liposomes in Mice Bearing C-26 Colon-Carcinoma. *Cancer Res.* **1992**, *52*, 6774–6781.
25. Venkatramu, V.; Falcomer, D.; Speghini, A.; Bettinelli, M.; Jayasankar, C. K. Synthesis and Luminescence Properties of Er^{3+}-doped $Lu_3Ga_5O_{12}$ Nanocrystals. *J. Lumin.* **2008**, *128*, 811–813.
26. Inasawa, S.; Sugiyama, M.; Yamaguchi, Y. Laser-Induced Shape Transformation of Gold Nanoparticles Below the Melting Point: The Effect of Surface Melting. *J. Phys. Chem. B* **2005**, *109*, 3104–3111.
27. Moghimi, S. M.; Szebeni, J. Stealth Liposomes and Long Circulating Nanoparticles: Critical Issues in Pharmacokinetics, Opsonization and Protein-binding Properties. *Prog. Lipid Res.* **2003**, *42*, 463–78.
28. Huynh, N. T.; Roger, E.; Lautram, N.; Benoit, J. P.; Passirani, C. The Rise and Rise of Stealth Nanocarriers for Cancer Therapy: Passive *versus* Active Targeting. *Nanomedicine* **2011**, *5*, 1415–33.